

Relaxation and electron transfer dynamics in bare and DTDCI sensitized MoS₂ nanoclusters

V. Chikan, M. R. Waterland, J. M. Huang, and D. F. Kelley

Citation: *The Journal of Chemical Physics* **113**, 5448 (2000); doi: 10.1063/1.1289765

View online: <http://dx.doi.org/10.1063/1.1289765>

View Table of Contents: <http://scitation.aip.org/content/aip/journal/jcp/113/13?ver=pdfcov>

Published by the [AIP Publishing](#)

Articles you may be interested in

[Controlled growth of vertically aligned MoO₃ nanoflakes by plasma assisted paste sublimation process](#)
J. Appl. Phys. **114**, 184310 (2013); 10.1063/1.4830278

[Investigation of the photoluminescence properties of thermochemically synthesized CdS nanocrystals](#)
AIP Advances **1**, 012113 (2011); 10.1063/1.3562892

[Carrier relaxation dynamics in annealed and hydrogenated \(GaIn\)\(NAs\)/GaAs quantum wells](#)
Appl. Phys. Lett. **87**, 252111 (2005); 10.1063/1.2149154

[Electron and hole trapping in WS₂ nanoclusters](#)
J. Chem. Phys. **113**, 793 (2000); 10.1063/1.481854

[Carrier trapping due to Fe³⁺/Fe²⁺ in epitaxial InP](#)
Appl. Phys. Lett. **70**, 3374 (1997); 10.1063/1.119175



Relaxation and electron transfer dynamics in bare and DTDCI sensitized MoS₂ nanoclusters

V. Chikan, M. R. Waterland, J. M. Huang,^{a)} and D. F. Kelley^{b)}
Department of Chemistry, Kansas State University, Manhattan, Kansas 66506-3701

(Received 8 May 2000; accepted 5 July 2000)

The trapping dynamics of photogenerated electrons and holes in MoS₂ nanoclusters has been studied using time resolved emission polarization and absorption spectroscopies. These results are compared to absorption kinetics obtained on MoS₂ nanoclusters with adsorbed DTDCI (DTDCI≡diethylthiodicarbocyanine iodide) dye. The results indicate that emission from the MoS₂ band edge state is polarized, while emission from trapped electrons and holes is unpolarized. This polarization difference is used to obtain the electron and hole trapping times and values of 275 ps and 42 ps, respectively, are obtained. Decays having the same time constants are observed in the transient absorption results. The results obtained on the MoS₂/DTDCI system show that electron injection occurs with a time constant of 12 ps. These kinetics also show a 225 ps decay component which is assigned to electron trapping and reverse electron transfer. The 225 ps decay time along with the 275 ps trapping time indicates that reverse electron transfer from the conduction band has a time constant of about 1.2 ns. Following trapping, reverse electron transfer from deep traps is slow. © 2000 American Institute of Physics. [S0021-9606(00)70337-0]

I. INTRODUCTION

There has recently been great interest in the sensitization of nanoporous semiconductor films and of semiconductor nanoclusters by adsorbed dyes.¹ Sensitization occurs when a dye absorbs light and injects an electron into the conduction band of a large band gap semiconductor. Much of this interest results from the potential application of these systems in solar energy conversion.²⁻⁶ Sensitization of nanoporous films exploits the fact that these materials have very high surface-to-volume ratios. In addition to high surface to volume ratios, some types of semiconductor nanoclusters and nanoporous films of these semiconductors exhibit quantum confinement of photogenerated electrons and holes. As a result of quantum confinement, the properties of the nanoclusters can be very different than the properties of the bulk. Potential applications of these materials may also exploit these differences.

Quantum confinement can have large effects on the spectroscopy and photophysics of semiconductor nanoclusters.⁷⁻¹⁰ The finite particle size can cause an increase in the band gap energy and cause the dense continua of valence and conduction band electronic states to become a set of delocalized, discrete states. In sufficiently small particles, the valence and conduction bands are replaced by sets of well-separated electronic states. In addition to these delocalized electronic states, semiconductor nanoclusters can also have a high density of localized surface states: electron

and hole traps. Thus nanometer sized semiconductor particles may have electronic structures which are vastly different than that of the bulk semiconductor, and can have correspondingly different photophysical and electronic properties. The finite relaxation rates of both electrons and holes between the delocalized and the localized (trap) states can dramatically affect the dynamics following direct photoexcitation or excitation of an adsorbed sensitizing dye.

The transition metal dichalcogenides, specifically MX₂ (M=Mo, W and X=S, Se) are of considerable interest in photoelectrochemical cells, principally because they are highly photostable.¹¹ Of these materials, nanoclusters of MoS₂ have received the most attention. Their synthesis, characterization, and several aspects of their spectroscopy have been reported.¹² MoS₂ is a layered material, consisting of covalently bound S–Mo–S trilayers separated by large van der Waals gaps. The molybdenum atoms are in trigonal bipyramidal sites between hexagonally close packed sulfur planes.^{13,14} MoS₂ nanoclusters are routinely synthesized using room temperature inverse micelle methods.¹² X-ray diffraction results show that aggregates of the particles have the same crystal structure as bulk MoS₂.^{12a} While there is no direct evidence regarding the morphology of these particles, comparison with analogous nanoclusters of materials having very similar bulk properties can yield some insight into this question. MoSe₂, WS₂, and WSe₂ have the same crystal structure as bulk MoS₂ and form comparably sized nanoclusters.¹³⁻¹⁷ Electron diffraction results show that MoSe₂, WS₂, and WSe₂ nanoclusters consist of single X–M–X trilayers having the same crystal structure as the bulk material.^{15,17} It is reasonable to assume that this is also the case for the smallest MoS₂ nanoclusters.

^{a)}Present address: NSF/Center for Micro-Engineered Materials, 203 Farris Engineering Center, University of New Mexico, Albuquerque, NM 87131.

^{b)}Author to whom correspondence should be addressed: Electronic mail: dfkelley@ksu.edu

In addition to structural and static spectroscopic studies, several types of dynamical studies have also been performed on MoS₂ nanoclusters.^{18–21} Specifically, dynamical studies of the recombination of trapped electrons and holes¹⁸ as well as interfacial electron transfer involving adsorbed electron acceptors have been reported.¹⁹ In addition, some of the interfacial electron transfer dynamics involving adsorbed dyes have also been studied.^{20,21}

In this paper, we examine the dynamics associated with direct photoexcitation of the nanoclusters and with electron injection from an adsorbed sensitizing dye, DTDCI (DTDCI≡diethylthiocarbocyanine iodide). These two sets of dynamics are considered together because both produce a conduction band electron which can subsequently undergo trapping and recombination with the hole or the oxidized dye. In the present study, time resolved emission polarization and adsorption measurements are used to determine these dynamics. We show that the band edge emission is polarized while emission from trapped electrons and holes is unpolarized and exploit these polarization differences to determine the trapping rates. However, trapping of either electrons or holes could result in partial or complete emission depolarization. Thus the observed depolarization dynamics may be primarily due to trapping of either carrier. This ambiguity can be resolved by the comparison of the emission depolarization and transient absorption results. This is because while both nanocluster and dye excitation result in injection of an electron into the nanocluster conduction band and subsequent electron trapping, no hole is produced and so there are no hole dynamics in the dye excitation case. The combination of these experiments permits determination of kinetics of electron injection, electron trapping, reverse (nanocluster to oxidized dye) electron transfer, and hole trapping.

The studies presented here use some of the same methods and are quite complementary to our recent studies of the electron and hole trapping dynamics in WS₂ nanoclusters. In previous publications^{15,16} we have shown that just as in the MoS₂ case, WS₂ bandedge emission is polarized while emission from trapped electrons and holes has little or no polarization. As in the present case, the emission depolarization undergoes a biphasic decay, and there is an ambiguity regarding which component corresponds to electron versus hole trapping. In the WS₂ case, this ambiguity was resolved by comparison of the dynamics in the presence and in the absence of adsorbed electron acceptors. The presence of the electron acceptors partially quenches the population of conduction band electrons, thereby allowing assignment of the electron trapping dynamics in the observed depolarization kinetics. We found that electron and hole trapping occur with 330 ps and 28 ps time constants, respectively. Comparable time scales are also observed in the MoS₂ case reported here. The results presented here also allow us to comment on the spectroscopy of MoS₂ nanoclusters.

The MoS₂/DTDCI results presented here can be compared to those obtained in our previous study of this system.²⁰ In that study, MoS₂/DTDCI was examined using transient absorption spectroscopy. However, the temporal resolution was 35 ps (compared to subpicosecond resolution here) and the signal to noise ratio was lower than in the

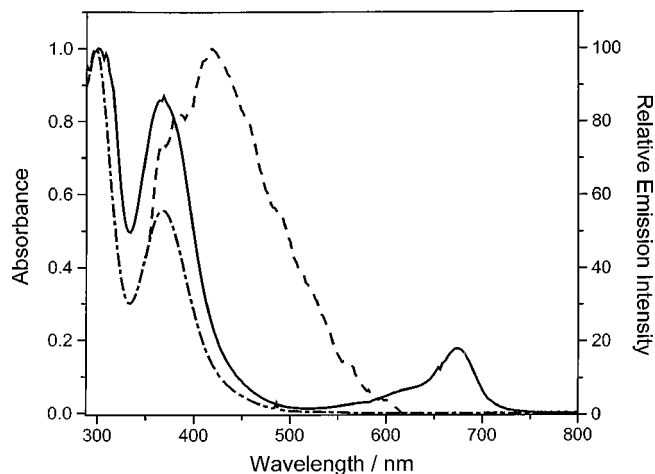


FIG. 1. Static absorption spectra of MoS₂ nanoclusters (dot-dash curve) and MoS₂ nanoclusters with adsorbed DTDCI dye (solid curve) in toluene. Also shown is an emission spectrum of MoS₂ nanoclusters in acetonitrile (dashed curve).

present study. Within these limitations, the results reported in the previous study are completely consistent with those reported here. However, the electron trapping process was not resolved and what is shown below to be reverse electron transfer from the conduction band was previously assigned to reverse electron transfer from shallow trap states.

II. EXPERIMENT

Molybdenum(IV)sulfide nanoclusters are synthesized using the same methods used in previous studies.^{12,18,19} Briefly, this synthesis is as follows. MoCl₄ is dissolved in a degassed ternary tridodecylmethyl ammonium iodide (TDAI)/hexanol/octane (8/8/84 by weight) inverse micelle solution, at a concentration of 1.0×10^{-3} M. Typical sample volumes are 10–20 mL. Four molar equivalents of H₂S are added via gas-tight syringe to these solutions. Reaction occurs within a few minutes. Following reaction, the inverse micelle solution along with the MoS₂ nanoclusters are extracted with an equal volume of acetonitrile. The nanoclusters partition between the nonpolar octane phase and the polar acetonitrile/TDAI/hexanol phase. The two phases show nearly identical absorption spectra, with a sharp absorption maximum at 364 nm (see Fig. 1). MoS₂ nanoclusters having a 364 nm absorption maximum have been characterized and have been reported to have an average diameter of 3.0 nm. In agreement with these results, we have recently performed rotational diffusion measurements on these particles and find an average diameter of about 3.5 nm. These rotational diffusion measurements have characterized the size distributions of these and several other types of nanoclusters, and will be reported in a later paper. The acetonitrile phase was used for emission polarization studies. Samples of MoS₂ nanoclusters with adsorbed DTDCI in toluene, hexane, or hexadecane were prepared by initially dissolving the dye in the nanocluster acetonitrile solution. This permits the DTDCI to attach to the nanoclusters.

The solvent is pumped off and the nanoclusters are then re-dissolved in hydrocarbon solvent. Bare nanocluster samples in toluene (without the dye) are prepared in exactly the same way.

Molybdenum(IV)chloride was synthesized by refluxing MoCl_5 in tetrachloroethylene in an evacuated and sealed vessel for three days. The resulting product was repeatedly washed with carbon tetrachloride in an inert atmosphere glovebox to remove starting material. TDAI was repeatedly washed with ether, and stored in the glovebox in the dark. Octane was distilled from sodium, in a nitrogen atmosphere. Acetonitrile was distilled from phosphorous pentoxide in a nitrogen atmosphere. Hexanol was distilled from iodine-activated magnesium in a nitrogen atmosphere. DTDCI was obtained from Exciton and used without further purification.

Time resolved emission results were obtained by time-correlated single photon counting, using an apparatus that has been previously described.²² In this apparatus, the sample is excited with 7 ps pulses from the second harmonic of a synch-pumped, cavity dumped cw dye laser (Spectra-Physics 3500), which is pumped by a cw mode locked YAG laser (Spectra-Physics 3800). Detection is accomplished with a Hamamatsu 6 μMCP PMT and time correlated single photon counting electronics. Wavelength selection is accomplished using a $\frac{1}{4}$ m monochromator with a 150 groove/mm grating. The emission kinetics reported here were taken at 450 nm, with a bandwidth of about 10 nm. In all cases, the excitation wavelength was 312 nm with pulse energies of about 1.0 nJ focused to a spot size of about 0.5 mm. This combination of low pulse energies and relatively large spot sizes results in fluences that are sufficiently low that multiphoton excitations are completely avoided. Polarized emission detection was accomplished using a 1 cm Glan-Taylor excitation polarizer and a Polaroid emission polarizer in a collinear geometry. Appropriate corrections were made for the polarization dependent throughput of the detection system.

The femtosecond transient absorption apparatus is based on a Clark-MXR CPA-2001 laser system. The CPA-2001 utilizes an Erbium doped fiber as the gain medium in a mode-locked fiber laser. The mode-locked output of the Erbium fiber oscillator, centered at 1550 nm, is pulse compressed and frequency-doubled to generate seed pulses for the Ti:Sapphire regenerative amplifier. This amplifier is pumped by a Q-switched, frequency-doubled Nd:YAG, which provides 8 W of 532 nm light at a repetition rate of 1 kHz. A feedback loop provides long-term Nd:YAG power stability. The resultant output is 800 μJ , 130 fs 775 nm pulses, at 1 kHz. This output is frequency doubled to 387.5 nm to provide sample excitation of the bare nanocluster samples. Alternatively, the 775 nm output is used to pump an optical parametric amplifier (Clark-MXR, Vis-OPA). This provides continuously tunable pump pulses with 10 μJ per pulse over the range from 420 nm to >660 nm. Nanocluster/dye samples were excited at 540 nm. Pump intensities are typically 20 $\mu\text{J}/\text{pulse}$ (387.5 nm) or 10 $\mu\text{J}/\text{pulse}$ (540 nm), and were typically focused to 0.5–1.0 mm spot sizes on a 1 cm thick sample cell. Sample concentrations are adjusted such that the absorbance at the excitation wavelength is 0.5–

1.0. The sample solutions are continuously stirred to avoid local heating effects. In all cases, reducing the intensity of the pump beam by a factor of 5 lowers the amplitude of the signal, but otherwise has no effect on the observed kinetics.

The sample is probed with a 10 nm slice of a white light continuum. Wavelength selection is accomplished using 10 nm bandpass interference filters. Continuum generation is achieved by focusing a small fraction (4%, ca. 32 μJ per pulse) of the 775 nm pulses onto a sapphire plate and then re-collimating with an achromat. A beam splitter separates the white light continuum into two components that form the reference and probe beams. Residual 775 nm from the continuum generation stage is removed prior to the sample. Residual pump energy is removed after the sample with a suitable dichroic mirror. In the present configuration, there is no compensation for group velocity dispersion, and the instrument response function is about 500 fs. Detection of the probe and reference beams is achieved with silicon photodiodes (UDT Detectors, model PIN-10D) biased at -12 V. The voltage from the photodiodes is amplified by a factor of either 100 or 200 and integrated with a Stanford Research Systems boxcar gated integrator. The resulting signals are input into a 16 bit A/D converter (Analog Devices, model PCI-MIO-16XE-50) in the backplane of a Pentium II PC running LabView. Each laser shot is integrated and digitized and all signal averaging is performed with home-written LabView software in the PC. Typically, a total of 5000 laser shots (20 scans \times 250 shots per point) are acquired at each delay stage position.

III. RESULTS AND DISCUSSION

A. Emission depolarization kinetics

The absorption spectra of MoS_2 nanoclusters with and without adsorbed DTDCI in room temperature toluene are shown in Fig. 1. The bare nanoclusters show an almost identical absorption spectrum in acetonitrile. The emission spectrum of MoS_2 nanoclusters in acetonitrile is also shown in Fig. 1. Following excitation with polarized 312 nm light, the resulting emission is polarized. The emission anisotropy is given by²³

$$r = (I_{\text{par}} - I_{\text{per}}) / (I_{\text{par}} + 2I_{\text{per}}), \quad (1)$$

where I_{par} and I_{per} are the emission intensities having polarizations parallel and perpendicular to that of the absorbed light, respectively. An experimental plot of the time-dependent 450 nm emission anisotropy of bare MoS_2 nanoclusters in acetonitrile is shown in Fig. 2. Photoselection theory shows that following excitation with polarized light, a linear oscillator exhibits an emission anisotropy of 0.40. The anisotropy starts out with a value close to 0.40 and subsequently decays, indicating that photoexcitation produces a state that is close to being a linear oscillator. Figure 2 shows that the anisotropy has an initial fast, almost pulse width limited decay, followed by a slower decay, on the hundreds

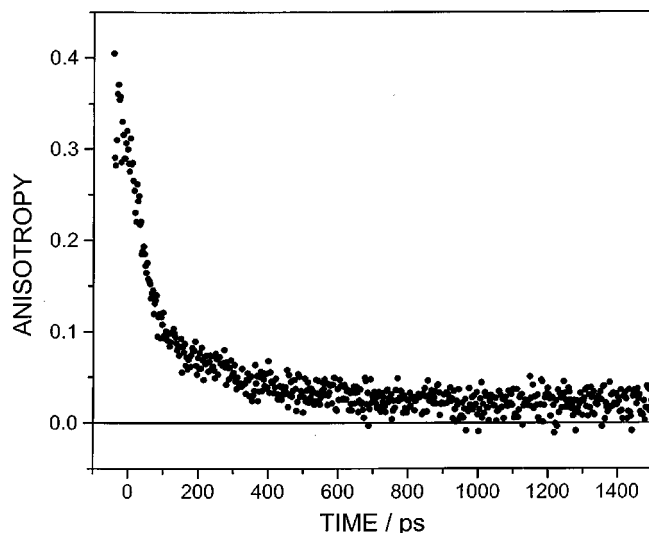


FIG. 2. Experimental plot of emission anisotropy versus time for MoS₂ nanoclusters in acetonitrile. The excitation and detection wavelength were 312 nm and 450 nm, respectively.

of picoseconds time scale. Figure 2 also shows that there is also a very small anisotropy which decays on a longer time scale.

These polarization results allow us to comment on the spectroscopy of MoS₂ nanoclusters, specifically, the assignment of the 364 nm peak. The 364 and 294 nm absorption peaks have previously been assigned¹² as correlating to the *A* and *B* excitons, respectively, in bulk MoS₂. The *A* and *B* exciton transitions are polarized in the plane of the nanoclusters,²⁴ perpendicular to the crystallographic *c*-axis. As such, the maximum anisotropy from excitation of the either the *A* or *B* exciton transition is 0.10. The observation of more polarized emission ($r \cong 0.40$ at $t=0$) indicates that this assignment is not correct and that the 364 nm peak correlates to a *c*-axis polarized transition of bulk MoS₂. Several such transitions have been observed at energies somewhat higher than the *A* exciton,^{25,26} but no definite assignment can be made at this point. This result indicates that the in plane transitions are subject to a larger quantum confinement effect than the out of plane transitions. Bulk MoS₂ has only a relatively weak interactions between S–Mo–S trilayers (along the *c*-axis), so this result is not too surprising. A similar conclusion was made in the WS₂ nanocluster case.^{15,16}

Analysis of the anisotropy decay, specifically the processes resulting in emission depolarization, is facilitated by plotting the results in terms of the kinetics of the polarized and unpolarized emission components. This corresponds to a model in which there are two emitting states, a linearly polarized ($r=0.40$) and an unpolarized, isotropic ($r=0.0$) oscillator. It is possible to relate the experimentally observed parallel and perpendicular emission intensities to the total emission intensities from the polarized and the unpolarized oscillators. Specifically,

$$I_{\text{par}} = I_{\text{par}, r=0.0} + I_{\text{par}, r=0.40}$$

and

(2a)

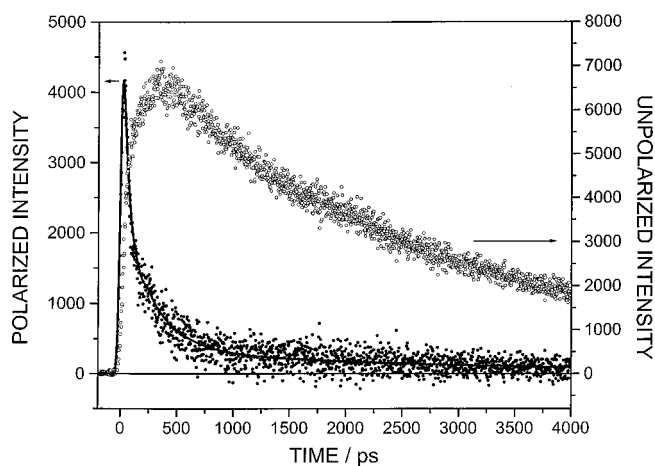


FIG. 3. Experimental plot of polarized emission intensity ($5/2(I_{\text{par}} - I_{\text{per}})$, closed circles) and of unpolarized emission intensity ($3/2(3I_{\text{per}} - I_{\text{par}})$, open circles) versus time for MoS₂ nanoclusters in acetonitrile. Also shown is a calculated triexponential decay which is convoluted with the instrument response function. The calculated curve corresponds to decay components and relative amplitudes of 42 ps (60%), 275 ps (35%) and 3.0 ns (5%).

$$I_{\text{per}} = I_{\text{per}, r=0.0} + I_{\text{per}, r=0.40}$$

Using Eq. (1) and an anisotropy value of 0.40 for the polarized oscillator, we get that

$$I_{\text{par}, r=0.40} = 3I_{\text{per}, r=0.40} \quad (2b)$$

For the unpolarized emission, $I_{\text{per}, r=0.0} = I_{\text{par}, r=0.0}$. The total population in each state is proportional to its total ($I_{\text{par}} + 2I_{\text{per}}$) time-dependent emission intensity. The total time-dependent polarized emission intensity is given by $I_{\text{tot}, r=0.40} = (I_{\text{par}, r=0.40} + 2I_{\text{per}, r=0.40}) = 5/2(I_{\text{par}} - I_{\text{per}})$, and the total unpolarized emission intensity is given by $I_{\text{tot}, r=0.0} = (I_{\text{par}, r=0.0} + 2I_{\text{per}, r=0.0}) = 3/2(3I_{\text{per}} - I_{\text{par}})$. Plots of these quantities are shown in Fig. 3. In the simplest case, these plots give the time dependent relative populations of the polarized and unpolarized emitting states. A state having emission which is partially polarized will contribute to the apparent intensities of both the polarized and unpolarized components. The extent of the contribution into each component will depend on the extent to which the emission is polarized. The strongly biphasic decays of the anisotropy (Fig. 2) and the polarized emission component in Fig. 3 indicate that there is an intermediate state which gives partially polarized emission. The emission anisotropy of this state can be estimated by extrapolating the slowly decaying (hundreds of picoseconds) component of the emission anisotropy to $t=0$, and a value of about $r=0.12$ is obtained. With the inclusion of this state, we get that the polarized emission intensity is related to the population in the $r=0.40$ oscillator plus some component of the $r=0.12$ oscillator. Similarly, the unpolarized emission intensity is related to the population in the isotropic ($r=0.0$) oscillator plus some component of the $r=0.12$ oscillator. Specifically,

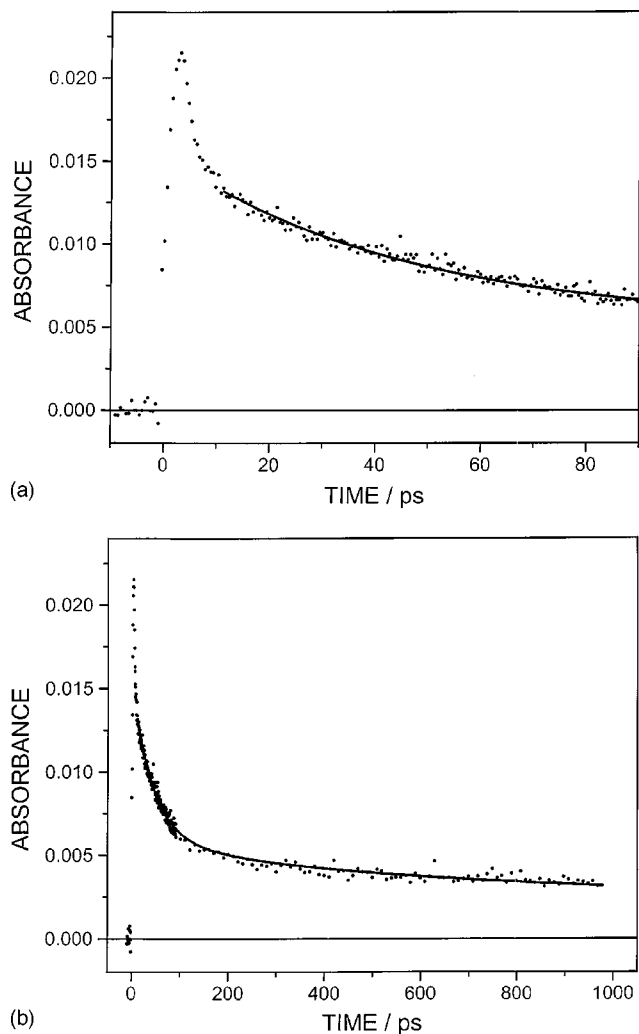


FIG. 4. Experimental plots of the absorption intensity versus time for MoS₂ nanoclusters in toluene. The excitation and probe wavelengths were 387.5 and 700 nm, respectively. A and B display the same results, but on different time scales. Also shown is a calculated curve corresponding to decay components of 42 ps (61%), 275 ps (17%) and 3.0 ns (22%).

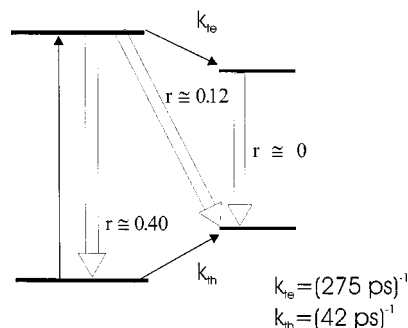
$$5/2(I_{\text{par}} - I_{\text{per}}) = I_{\text{tot}, r=0.40} + 0.3I_{\text{tot}, r=0.12}, \quad (3a)$$

$$3/2(3I_{\text{per}} - I_{\text{par}}) = I_{\text{tot}, r=0.0} + 0.7I_{\text{tot}, r=0.12}. \quad (3b)$$

To the extent that the oscillator strengths and spectral characteristics of these oscillators are the same, the relative emission intensities shown in Fig. 3 are related to the relative populations. Figure 3 shows that the polarized [$5/2(I_{\text{par}} - I_{\text{per}})$] kinetics exhibit an instrument limited rise followed by a triexponential decay. These kinetics are fit to components having decay times and relative amplitudes of 42 ps (65%), 275 ps (30%) and 3.0 ns (5%). The corresponding unpolarized emission kinetics are also shown in Fig. 3. There are two kinetic components having finite rise times followed by a multiexponential decay. The slower of the two rise times occurs on the timescale of a few hundred picoseconds, and is associated with the 275 ps decay of the polarized emission. Most of the unpolarized emission has a rise time which matches the fast (42 ps) decay of the polarized emission.

The initial polarized emission is assigned to the band-edge state and the unpolarized emission is assigned to emission from trapped electrons and holes. The long-time multiexponential decay of the unpolarized emission is associated with the distribution of trapped electron-hole separations, and has been previously discussed for both MoS₂ and WS₂ nanoclusters.^{15,19} The intermediate state is assigned to trapped holes and conduction band electrons. With these assignments, the unpolarized emission is due to trapped holes recombining with trapped electrons and to a lesser extent, conduction band electrons, and the polarized emission is due to conduction band electrons recombining with valence band holes, and to a lesser extent, trapped holes. The extent to which the band edge, trapped hole/conduction band electron, and trapped electron and hole states contribute to the polarized and unpolarized emission components is given by Eq. (3). Thus the 42 ps and 275 ps depolarization components are assigned to hole and electron trapping, respectively. It follows that the band-edge emission is polarized as a linear oscillator, $r=0.40$, and that hole trapping significantly, but not completely, depolarizes this emission. Radiative recombination of a trapped hole and a conduction band electron gives somewhat polarized ($r=0.12$) emission. This situation is depicted in Scheme 1.

Scheme 1



The assignment of comparatively rapid hole trapping followed by slower electron trapping (rather than the other way around) is established by comparison to the transient absorption results obtained on MoS₂ nanoclusters with and without adsorbed dyes. These results are discussed below. The small ($\sim 5\%$), long lived component of polarized emission may be due to nanoparticles lacking trap states, a small polarization from trapped electrons and holes, or thermal population of the conduction band from trapped electrons. These possible contributions to the long lived polarized emission are not mutually exclusive, and we find that the exact amount of this component varies from sample to sample. In the case of WS₂ nanoclusters, it was shown that the electron traps are very shallow and the hole traps are much deeper. Thus in the WS₂ case, a similar long lived polarized emission component is at least in part due to thermal repopulation of the conduction band by trapped electrons.¹⁶ No effort to further analyze this component is made here.

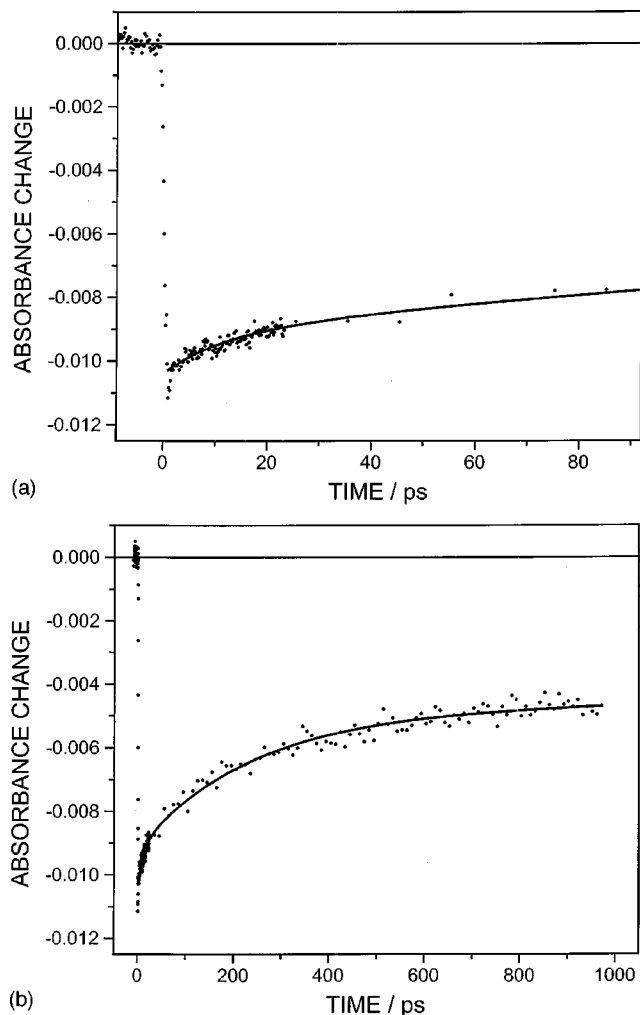


FIG. 5. Experimental plots of the absorption intensity versus time for MoS₂ nanoclusters with adsorbed DTDCI in toluene. The excitation and detection wavelengths were 540 and 660 nm, respectively. A and B display the same results, but on different time scales. Also shown is a calculated curve corresponding to decay components of 12 ps, 225 ps, 1.7 ns and a long lived absorption.

B. Transient absorption kinetics

The 700 nm transient absorption kinetics of MoS₂ nanoclusters following 387.5 nm excitation are shown in Fig. 4. Several kinetic components can be seen. There is a fast transient observed in the first 10 ps. This consists of an approximately 1.5 ps rise followed by a 2.5–3.0 ps decay. This transient is associated with relaxation to the bandedge, indicating that the state excited with 387.5 light is not the band edge state. This suggests that the emitting bandedge state corresponds to a weak absorption buried under the red edge of the 364 nm absorption. The emission polarization results indicate that the excited and emitting states are both polarized parallel the *c*-axis but no detailed assignment of these states can be made on the basis of the results presented here.

The fast transients are followed by a decay having components of 42 ps (61%), 275 ps (17%) and 3 ns (22%). A calculated curve corresponding to these values is also shown in Fig. 4. These decay times correspond to the times observed in the polarized emission kinetics discussed above.

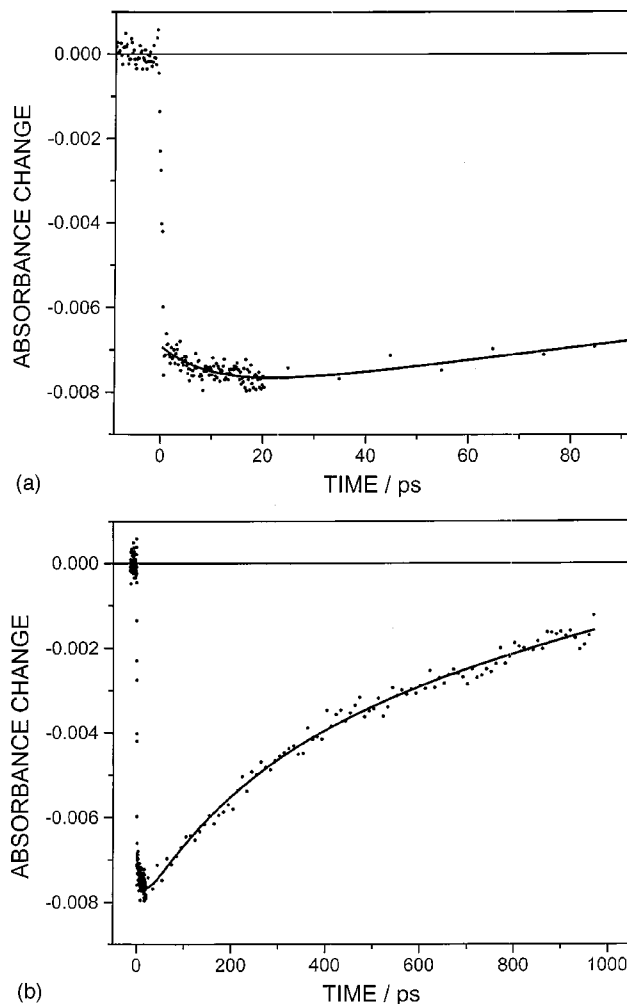


FIG. 6. Same as Fig. 5, except the detection wavelength was 700 nm.

The relative amplitudes of these transients indicate that hole trapping results in considerable loss of 700 nm absorption, and that electron trapping also results in loss of 700 nm absorption, but to a lesser extent.

The 660 nm and 700 nm transient absorption kinetics of MoS₂ nanoclusters with adsorbed DTDCI dye following 540 nm excitation are shown in Figs. 5 and 6, respectively. Several species can absorb in this wavelength range and may therefore contribute to the observed kinetics. DTDCI has a significant ground state absorption at 660 and 700 nm (see Fig. 1) and the net absorbance change following photoexcitation is negative; the ground state dye is bleached. In addition to the ground state bleach, there can be absorption from the excited state dye, the dye cation, and the conduction band or trapped electron. Following the pulse width limited onset of the bleach, the 660 nm kinetics show a subsequent small amplitude, 12 ps increase in the absorption (a bleach decrease) followed by a slower bleach decay. The 700 nm kinetics also show a small amplitude initial 12 ps transient, but at this wavelength it is an absorption decrease (an apparent increase of the bleach). Figure 4 shows that the bare MoS₂ kinetics exhibit no 12 ps transient, so this kinetic component is assigned to an interaction of the nanocluster with the dye. Cyanine dyes are known to inject electrons into semiconduc-

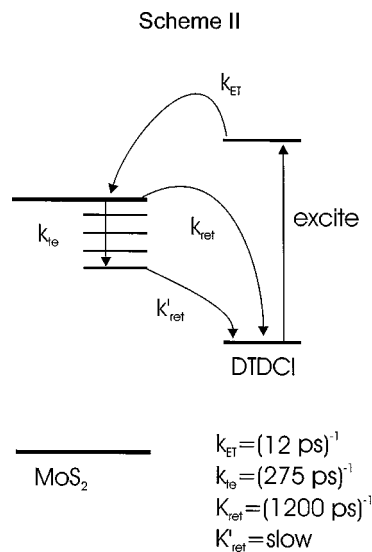
tors and it is quite reasonable to assign the 12 ps transient to electron injection from the photoexcited dye to the nanocluster conduction band. With this assignment, it follows that the excited state dye has less absorbance than the dye cation and the conduction band electron at 660 nm. The opposite is true at 700 nm. Almost identical results are obtained in hexane and in hexadecane solvents.

Cyanine dyes are known to undergo excited state isomerization,^{27–29} with a rate that depends on the solvent viscosity. This isomerization results in a time dependent increase in the observed bleach throughout the 600–700 nm region for free DTDCI in alcohols. Otherwise stated, throughout this spectral region, the excited state dye has more absorbance prior to, compared to following isomerization. We find that the isomerization rates vary from about 30 ps in ethanol to about 80 ps in an ethanol/ethylene glycol mixture. Identical 12 ps transients are obtained for MoS₂/DTDCI in hexane and hexadecane solvents, which have viscosities differing by about a factor of 10. Thus no solvent viscosity dependence of the 12 ps transient seen in the MoS₂/DTDCI system, indicating that it not associated with DTDCI isomerization. If isomerization were involved in this transient, then a large solvent viscosity effect would be expected. The photoisomerization involves torsion of the methylene chain and we conclude that this does not occur when the dye is adsorbed on the nanoparticles.

Following the 12 ps transient, at both wavelengths there is a slower, 225 ps decay as well as a long lived, nanosecond absorbance change. The most important thing to note in Figs. 5 and 6 is that no 42 ps component is observed in the MoS₂/dye transient absorption kinetics. This establishes that the 42 ps transients seen in the polarized emission kinetics and in the bare nanocluster absorption kinetics are not related to the electron dynamics and may therefore be assigned to hole trapping.

Several kinetic components can be extracted by fitting the decays in Figs. 5 and 6. This fitting is complicated by the observation that these samples show weak DTDCI emission, about 12% of the emission intensity seen in ethanol solution. This indicates that about 12% of the dyes do not undergo electron transfer but simply radiate, presumably with their 1.7 ns solution phase lifetime. The 660 nm calculated curve also has a 12% component of 1.7 ns bleach decay associated with dyes that do not inject. Inclusion of this 1.7 ns (12%) component assumes that the extinction coefficient of the excited state dye is small compared to that of the ground state dye at these wavelengths. DTDCI has significant emission intensity at 700 nm, and the 700 nm kinetics show a somewhat larger 1.7 ns component due to stimulated emission. Despite this complication, both 660 nm and 700 nm curves clearly show a 225 ps component. The 225 ps bleach recovery transient observed here is significantly shorter than the 275 ps decays observed in the emission polarization and the bare nanocluster absorption kinetics. It is also of interest to note that electron trapping causes an absorption decrease in the bare nanocluster case (Fig. 4), while the 225 ps transient in the nanocluster/dye case is an increase of the absorbance (i.e., a decrease in the intensity of the bleach). This indicates partial repopulation of the ground state dye from the conduc-

tion band electron. The 660 and 700 nm extinction coefficients of the ground state dye are very large and partial repopulation of the ground state dye is expected to result in a net increase of the absorption, consistent with the observed decays. Thus reverse (conduction band to oxidized dye) electron transfer occurs along with electron trapping. These dynamics are summarized in Scheme 2.



From the difference of the bare nanocluster and nanocluster/dye conduction band decays, it is possible to estimate the rates of conduction band reverse electron transfer, k_{ret} . These values (275 ps and 225 ps, respectively) give an estimate for k_{ret}^{-1} of about 1.2 ns. This value comes from taking the difference of two separate rates and is therefore subject to considerable uncertainty. The above rate constants indicate that about 20% of the conduction band electrons undergo reverse electron transfer, while about 80% get trapped. Following electron trapping, reverse electron transfer from trap states, k'_{ret} , occurs on a longer time scale and is not apparent in the kinetics presented here.

The results presented here show that electron trapping occurs much more slowly than hole trapping. It may be possible to rationalize this result in terms of the trapping reorganization energy and the extent of electron-phonon coupling. The small magnitude of electron-phonon coupling results from the nature of the bonding in MX₂-type compounds.²⁴ Optical excitation for these materials is largely a metal centered *d-d*, nonbonding-to-nonbonding, transition. As a result, photoexcitation produces very little lattice distortion and there is very little electron-phonon coupling associated with band gap excitation. If electron or hole trapping significantly distorts the local lattice, then there is a considerable reorganization energy associated with this process. In the case of WS₂ nanoclusters, we recently showed that electron traps are very shallow (a few hundred wave numbers), and hole traps are considerably deeper (a few thousand wave numbers).^{15,16} In a simple exciton model of the traps, this difference is due to the different carrier effective masses and the same situation is probably the case in MoS₂ nanoclusters. We speculate that in the case of electron trapping, the shallow traps along with the lattice distortion result in small Franck–Condon factors for electron trapping.

In other words, the significant reorganization energy and small trapping energy results in an energetic barrier to electron trapping. Hole traps are much deeper and the barrier may be smaller in this case. This is basically a Marcus Theory consideration.³⁰ The barrier for electron or hole trapping is given by

$$\Delta G^\ddagger = \lambda/4(1 + \Delta G/\lambda)^2, \quad (4)$$

where λ is the reorganization energy and ΔG is the trapping energy. Equation (4) shows that if λ is comparatively large and ΔG is small, then there is a significant barrier to trapping. As the trapping energy gets larger and approaches the same magnitude as the reorganization energy, the barrier gets smaller and the trapping rate gets larger. We also note that the electron and hole trapping times reported here are considerably longer than what is observed in other nanocluster systems such as SnO₂, TiO₂, Fe₂O₃, and most notably, CdS and CdSe.^{31–40} We speculate that the reason that slow trapping is observed in MoS₂ and WS₂ nanoclusters is related to the weak electron-phonon coupling in these materials. However, electronic factors may also be important in determining the trapping rates and the slow trapping observed in MoS₂ and WS₂ nanoclusters may also be due to electronic overlap considerations. The roles of electronic and vibrational factors in controlling trapping rates in MoS₂ and WS₂ nanoclusters are not clear at this point.

There have been numerous studies of electron injection from adsorbed dyes into semiconductors. The injection rates depend on the energetics, the extent of the electronic coupling and the density of conduction band electronic states at the injection energy. A wide range of electron transfer times are observed, ranging from less than a picosecond to hundreds of picoseconds. We are currently studying the electron injection rates from DTDCI and other cyanine dyes in closely related nanocluster systems to assess the roles of each of these factors in determining the electron injection rates. Those results will be reported in a later paper.

IV. CONCLUSIONS

Several conclusions can be drawn from the results presented here.

- (1) MoS₂ nanoclusters exhibit polarized emission from the bandedge state and unpolarized emission from trapped electrons and holes. This polarization difference can be used to determine the rates of electron and hole trapping. Such determinations are not possible from the total (unpolarized) emission kinetics. We find that hole and electron trapping times are 42 ps and 275 ps, respectively.
- (2) The same decay times seen in the polarized emission kinetics are also seen in the transient absorption kinetics. In addition, faster rise and decay components are also seen in the transient absorption results. These transients correspond to relaxation to the band edge state, but no definite assignments can be made at this time.
- (3) Electron injection from adsorbed DTDCI to the MoS₂ nanocluster conduction band occurs with a 12 ps time constant following dye photoexcitation. This is followed by a 225 ps decay which is assigned to electron trapping and reverse electron transfer from the conduction band. The presence of this 225 ps decay and the absence of a 42 ps decay permits the assignment of the electron trapping decay component seen in the polarized emission and bare nanocluster transient absorption results. From these rates, the reverse electron transfer time is inferred to be about 1.2 ns. This means that about 20% of the conduction band electrons undergo reverse electron transfer, while about 80% get trapped.
- (4) Following electron trapping, reverse electron transfer from these deep traps is slow and occurs on the nanosecond time scale.

ACKNOWLEDGMENTS

This work was supported by a grant from the Department of Energy. M.R.W. also thanks the Foundation for Research, Science and Technology of New Zealand for a New Zealand Science and Technology Postdoctoral Fellowship (Contract No. KSU-901).

- ¹For a recent and comprehensive review see: *Semiconductor Nanoclusters—Physical, Chemical and Catalytic Aspects*, edited by P. V. Kamat and D. Meisel (Elsevier, New York, 1997).
- ²A. Hagfeldt and M. Gratzel, *Chem. Rev.* **95**, 49 (1995).
- ³M. K. Nazeeruddin, A. Kay, I. Rodicio, R. Humphry-Baker, E. Muller, P. Liska, N. Vlachopoulos, and M. Gratzel, *J. Am. Chem. Soc.* **115**, 6382 (1993).
- ⁴T. Hannappel, B. Burfeindt, W. Storck, and F. Willig, *J. Phys. Chem.* **101**, 6799 (1997).
- ⁵S. K. Deb, R. Ellingson, S. Ferrere, A. J. Frank, B. A. Gregg, A. J. Nozik, N. Park, and G. Schlichthorl, presented at the 2nd World Conference on Photovoltaic Solar Energy Conversion, July 1998, Vienna, Austria.
- ⁶S. K. Deb, S. Ferrere, A. J. Frank, S. K. Huang, A. J. Nozik, G. Schlichthorl, and A. Zaban, presented at the 26th IEEE Photovoltaic Specialists Conference, October, 1997, Anaheim, California.
- ⁷L. E. Brus, *J. Phys. Chem.* **90**, 2555 (1986).
- ⁸R. Rosetti, J. E. Ellison, J. M. Gibson, and L. E. Brus, *J. Chem. Phys.* **80**, 4464 (1984).
- ⁹M. V. Rama Krishna and R. A. Friesner, *J. Chem. Phys.* **95**, 8309 (1991).
- ¹⁰P. E. Lippens and M. Lannoo, *Phys. Rev. B* **39**, 10935 (1989).
- ¹¹H. Gerischer, in *Topics in Applied Physics*, Vol. 31: Solar Energy Conversion, edited by B. O. Seraphin (Springer, Berlin, 1979).
- ¹²(a) J. P. Wilcoxon and G. A. Samara, *Phys. Rev. B* **51**, 7299 (1995); (b) J. P. Wilcoxon, P. P. Newcomer, and G. A. Samara, *J. Appl. Phys.* **81**, 7934 (1997).
- ¹³F. Levy, *Crystallography and Crystal Chemistry of Materials with Layered Structures* (Reidel, Holland, 1976), p. 2.
- ¹⁴*Electrons and Phonons in Layered Crystal Structures*, edited by T. J. Wieting and M. Schluter (Reidel, Holland, 1979).
- ¹⁵J. M. Huang, R. Laitinen, and D. F. Kelley, *Phys. Rev. B* (in press).
- ¹⁶J. M. Huang and D. F. Kelley, *J. Chem. Phys.* **113**, 793 (2000).
- ¹⁷J. M. Huang and D. F. Kelley, *Chem. Mater.* (in press).
- ¹⁸F. Parsapour, D. F. Kelley, S. Craft, and J. P. Wilcoxon, *J. Chem. Phys.* **104**, 4978 (1996).
- ¹⁹R. Doolen, R. Laitinen, F. Parsapour, and D. F. Kelley, *J. Phys. Chem. B* **102**, 3906 (1998).
- ²⁰C. I. Butoi, B. T. Langdon, and D. F. Kelley, *J. Phys. Chem. B* **102**, 9635 (1998).

- ²¹B. T. Langdon, V. J. MacKenzie, D. J. Asunskis, and D. F. Kelley, *J. Phys. Chem. B* **103**, 11176 (1999).
- ²²M. R. Nimlos, M. A. Young, E. R. Bernstein, and D. F. Kelley, *J. Chem. Phys.* **91**, 5268 (1989).
- ²³A. Albrecht, *J. Mol. Spectrosc.* **6**, 84 (1961).
- ²⁴R. Coehoorn, C. Haas, J. Dijkstra, C. J. F. Flipse, R. A. deGroot, and A. Wold, *Phys. Rev. B* **35**, 6195 (1987); R. Coehoorn, C. Haas, and R. A. deGroot, *ibid.* **35**, 6203 (1987).
- ²⁵W. Y. Liang, *J. Phys. C* **6**, 551 (1973).
- ²⁶A. R. Beal, W. Y. Liang, and H. P. Hughes, *J. Phys. C* **9**, 2449 (1976); A. R. Beal and H. P. Hughes, *ibid.*, **12**, 881 (1979).
- ²⁷Y. Onganer, M. Yni, D. R. Bessire, and E. L. Quitevis, *J. Phys. Chem.* **97**, 2344 (1993).
- ²⁸R. E. Di Paolo, L. B. Scaffardi, R. Duchowicz, and G. M. Bilmes, *J. Phys. Chem.* **99**, 13796 (1995).
- ²⁹A. K. Chibsov, G. V. Zakharova, H. Gorner, Y. A. Sogulyaev, I. L. Mushkalo, and A. I. Tolmachev, *J. Phys. Chem.* **99**, 886 (1995).
- ³⁰R. A. Marcus, *J. Chem. Phys.* **43**, 679 (1965); *Annu. Rev. Phys. Chem.* **15**, 155 (1964); J. Jortner and M. Bixon, *J. Chem. Phys.* **88**, 167 (1988).
- ³¹V. I. Klimov, Ch. J. Schwarz, D. W. McBranch, C. A. Leatherdale, and M. G. Bawendi, *Phys. Rev. B* **60**, R2177 (1999).
- ³²V. I. Klimov and D. W. McBranch, *Phys. Rev. Lett.* **80**, 4028 (1998).
- ³³N. P. Ernsting, M. Kaschke, H. Weller, and L. Katsikas, *J. Opt. Soc. Am. B* **7**, 1630 (1990); Y. Kayanuma, *Phys. Rev. B* **38**, 9797 (1988).
- ³⁴P. Guyot-Sionnest, M. Shim, C. Matranga, and M. Hines, *Phys. Rev. B* **60**, R2181 (1999).
- ³⁵P. Guyot-Sionnest and M. A. Hines, *Appl. Phys. Lett.* **72**, 686 (1998).
- ³⁶D. E. Skinner, D. P. Colombo, Jr., J. J. Cavaleri, and R. M. Bowman, *J. Phys. Chem.* **99**, 7853 (1995).
- ³⁷J. J. Cavaleri, D. P. Colombo, Jr., and R. M. Bowman, *J. Phys. Chem.* **102**, 1341 (1998).
- ³⁸J. Z. Zhang, R. H. O'Neil, T. Roberti, J. L. McGowen, and J. E. Evans, *Chem. Phys. Lett.* **218**, 479 (1994).
- ³⁹J. Z. Zhang, R. H. O'Neil, and T. W. Roberti, *J. Phys. Chem.* **98**, 3859 (1994).
- ⁴⁰N. J. Cherepy, D. B. Liston, J. A. Lovejoy, H. Deng, and J. Z. Zhang, *J. Chem. Phys. B* **102**, 770 (1998).